SolarPACES 2024, 30th International Conference on Concentrating Solar Power, Thermal, and Chemical Energy Systems

Solar Fuels and Chemical Commodities

https://doi.org/10.52825/solarpaces.v3i.2366

© Authors. This work is licensed under a Creative Commons Attribution 4.0 International License

Published: 22 Sep. 2025

Volumetric Absorption of Direct and Indirect Radiation in Porous Redox Structures for Solar Fuel Production

Louis Thomas[1,2,*], Stefan Brendelberger[1], Robin Tim Broeske[1], Martin Roeb[1], and Christian Sattler[1,2]

[1]German Aerospace Center (DLR), Germany

[2]RWTH Aachen University, Germany

*Correspondence: Louis Thomas, louis.thomas@dlr.de

Abstract. In order to reduce the dependency on fossil fuels and thereby the emission of greenhouse gases, the large-scale production of renewable chemical energy carriers plays an important role. Here, the production of green hydrogen via solar thermochemical redox cycles presents a promising pathway. In order to develop and improve reactor concepts that utilize this approach, the usage of numerical models is essential. The volumetric radiation absorption within porous redox structures is often simplified or neglected within such models. Furthermore, the setup of redox structure and radiation source is often limited to the direct collimated irradiation of flat structures. Therefore, a Monte-Carlo ray-tracing model is developed to simulate the volumetric radiation absorption within porous redox structures of different geometries and reactor boundary conditions. In addition to the direct irradiation of a flat geometry with collimated solar radiation, the indirect diffuse irradiation of a cylindrical redox structure is evaluated. The model setup and resulting absorption profiles are presented here and will serve as an input to material models for heat transfer simulations.

Keywords: Solar Thermochemistry, Ceria Redox Cycle, Reticulated Porous Ceramics, Radiation Modeling, Volumetric Absorption

Table 1. *Nomenclature*

Symbols		**Abbreviations**	
F	View factor [-]	abs	Absorbed
l	Path length [m]	em	Emitted
N	Number [-]	ox	Oxidation
$\dot{Q}$	Power [W]	red	Reduction
r, t	Radius, Thickness [m]	RPC	Reticulated porous ceramics
T	Temperature [K]		
Greek symbols			
α	Absorptivity [-]		
β	Extinction coefficient [m^{-1}]		
δ	Reduction extent [-]		
η	Share; Fraction [-]		

1. Introduction

In order to significantly reduce $\mathrm{CO_2}$ emissions and tackle the climate crisis, a fast decarbonization of the industry and transport sector is essential. The utilization of renewable chemical energy carriers and fuels such as hydrogen is a crucial step in order to reduce the dependency on fossil fuels [1]. Solar driven thermochemical redox cycles pose a promising pathway for the production of renewable chemical commodities and fuels [2]. The two-step $\mathrm{CeO_{2-\delta}}$ redox cycle is one approach that can use solar energy to heat the redox material to high temperatures ($\approx 1773\ \mathrm{K}$), partially reducing the material and releasing oxygen in an endothermic process (formula 1). In a second step the material is cooled down ($\approx 1200\ \mathrm{K}$) and brought into contact with water vapor. This triggers an exothermic reaction that splits the water and releases hydrogen in the process (formula 2) [3]. The reduction extent δ strongly increases with the redox material temperature and depends on the oxygen partial pressure in the reactor environment. Reaching high reduction extent changes $\Delta\delta$ between reduction and oxidation step enhances the overall water splitting reaction and thereby the hydrogen production.

$$\mathrm{CeO_{2-\delta_{ox}}} \rightarrow \mathrm{CeO_{2-\delta_{red}}} + \frac{\Delta\delta}{2}\mathrm{O_2} \tag{1}$$

$$\mathrm{CeO_{2-\delta_{red}}} + \Delta\delta\mathrm{H_2O} \rightarrow \mathrm{CeO_{2-\delta_{ox}}} + \Delta\delta\mathrm{H_2} \tag{2}$$

$\mathrm{CeO_{2-\delta}}$ in form of reticulated porous ceramics (RPC) is used as redox material in state-of-the-art fixed bed receiver-reactors [4]. The open pore structure allows the incoming radiation to enter into the material volume, as well as water vapor to permeate into the bulk material. The RPC elements are often in the form of fairly flat block structures covering the inner reactor walls, where they are irradiated directly by concentrated solar radiation during the reduction step. This configuration however leads to large temperature gradients within the structure [5]. Mass fractions of the material that do not reach sufficiently high temperatures are only slightly reduced and therefore contribute hardly to the water splitting process. Additionally, parts of the RPC structure on the directly irradiated site can overheat and get damaged in the process.

In order to address these challenges, new reactor concepts and redox material structures are investigated. The solar interface of the reactor is one important characteristic that influences the temperature profile within the redox structure. Furthermore, the geometry and morphology of the redox material itself can be altered and needs to be tailored to the reactor boundary conditions. For the state-of-the-art fixed bed receiver-reactors hierarchically ordered

3D-printed redox structures are investigated as an alternative to the directly irradiated flat isotropic RPC elements [5, 6]. Furthermore, a multi aperture receiver-reactor with cylindrical redox structures that are heated primarily by indirect thermal radiation has been proposed recently [7].

In order to develop and assess receiver-reactors and redox structures different numerical models for selected reactor and material designs have been developed with relatively detailed representations of the reactor geometry [8, 9]. These models are therefore computationally costly while the redox material is implemented with homogeneous, isotropic properties. For investigations applying large scale parameter studies, more generic and simplified reactor models are required. Amongst others, receiver-reactors with 1D representations of the redox structures and with homogenized material properties have been used in such models [7, 10]. One aspect that needs to be considered in the models is the absorption of external radiation. For complex structures, material properties and reactor boundary conditions no analytical models are available. An accurate estimation of the volumetric radiation absorption needs dedicated investigations or model simplifications are required. For example, in a recent study the radiation exchange of cylindrical RPC's with hot reactor cavity walls has been simplified by assuming an artificial thin opaque layer surrounding the redox structure [7]. This simplification avoids the challenges of modeling the volumetric absorption, but leads to a conservative estimation of the material performance due to higher resulting temperature gradients. In order to have a more realistic approximation of these cases, a Monte-Carlo ray-tracing model is developed that allows to locally resolve the radiation exchange for less constrained cases. In the following the model is described and the volumetric absorption profiles are presented for different RPC geometries (flat and cylinder), material properties (reduction extent and extinction coefficient) and boundary conditions (direct collimated and indirect diffuse irradiation).

2. Method

2.1 Model setup

The Monte-Carlo ray-tracing model presented here is implemented in Python and assumes geometrical optics and neglects diffraction effects at surfaces. Optical and structural properties of the porous redox structure are described by effective isotropic properties taken from literature (table 2), i.e. no pore level geometry is modeled. For redox structures in receiver-reactors operated under reduced total pressure a participating fluid medium is neglected. Individual rays travel on straight paths through the RPC structure until they interact with the material. Free path lengths l_{ray} are calculated using the Beer-Lambert-Law with the extinction coefficient β_{RPC} of the RPC structure and a random number $U_{i,1}$ (formula 3). At the interaction points the type of interaction with the RPC structure (absorption or reflection) is determined based on the local absorptivity α of $\mathrm{CeO_{2\text{-}\delta}}$ (formula 6), which in turn depends on the reduction extent and temperature [11], and the random number $U_{i,4}$. For reflected rays, new ray directions are sampled as 3D normalized vectors using spherical coordinates and the random numbers $U_{i,2}$ and $U_{i,3}$ (formula 4, 5). Ray interactions, absorption and scattering events, within the structure are recorded per spatial element of the RPC structure. Material properties can be defined locally, however for the simulations presented below constant material properties are used. Individual pseudo-random number sampling from a uniform distribution ($U_{i,j} \in U[0,1]$) for ray path lengths, directions and type of interaction is implemented using the Python NumPy BitGenerator PCG-64. The setup of the model is depicted as a flow chart in figure 1.

$$l_{\mathrm{ray}} = -\ln\frac{U_{i,1}}{\beta_{\mathrm{RPC}}} \tag{3}$$

$$\theta = cos^{-1}\left(2U_{i,2} - 1\right) \in [0,\, \pi], \qquad \varphi = 2\pi U_{i,3} \in [0,2\pi] \tag{4}$$

$$\hat{\boldsymbol{v}}_{\text{direction}} = [sin(\theta)\,cos(\varphi)\,, sin(\theta)\,sin(\varphi)\,, cos(\theta)] \tag{5}$$

$$U_{i,4} \rightarrow \begin{cases} U_{i,4} \leq \alpha_{CeO_{2-\delta}} \rightarrow \text{ray absorbed} \\ U_{i,4} > \alpha_{CeO_{2-\delta}} \rightarrow \text{ray reflected} \end{cases} \tag{6}$$

$$r_{\text{cavity}} = \sqrt{\left(\frac{\pi r_{\text{RPC}}^2}{\eta_{\text{surf,max}}}\right)} - 2r_{\text{RPC}} \tag{7}$$

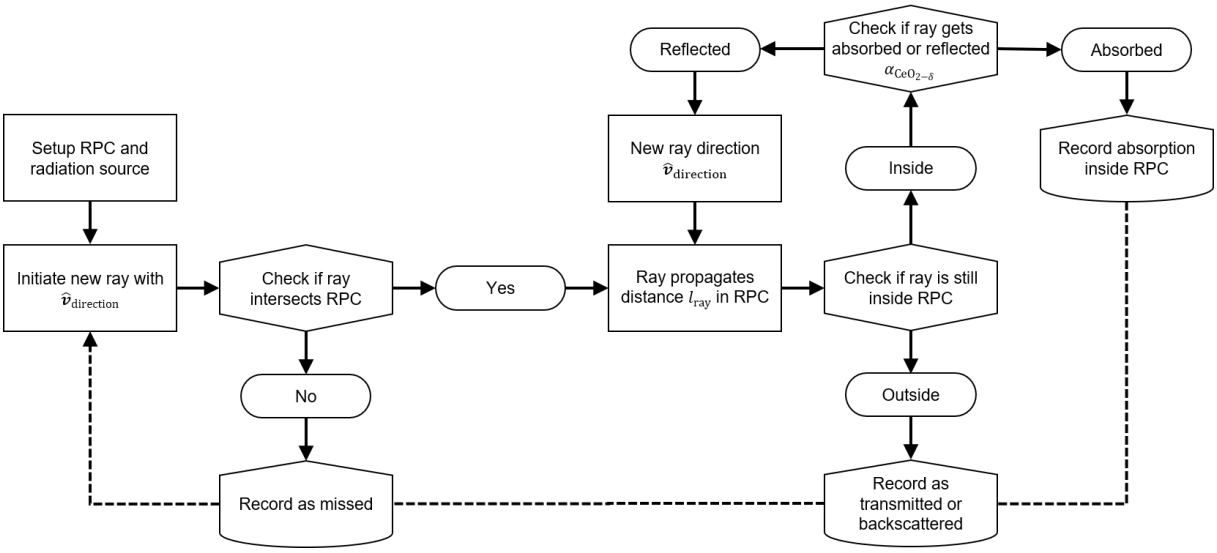

Figure 1. *Flow chart visualizing the Monte-Carlo ray-tracing model. Simulations start with the setup of the RPC and radiation source (left) and iterates through the following steps until a ray is absorbed by the RPC or left the structure, then a new ray is initiated.*

For the state-of-the-art receiver-reactor case, the redox material is modeled as a flat structure with thickness t_{RPC} and collimated radiation impinging on one side (figure 2a). Radiation leaving the structure on the other side is considered as missed. The volumetric absorption per element is recorded relative to the total incoming radiation. In order to obtain absolute values for successive heat transfer calculations, this value needs to be scaled accordingly. Collimated rays reach the flat RPC perpendicular to the surface. The radiation source for the indirect irradiated case is implemented as a concentric cylindrical surface around the RPC cylinder as a simplified model for a homogeneous reactor cavity environment (figure 2b). The radiation source is assumed to be a perfect Lambertian emitter at constant temperature, where the emitted power of each individual ray depends on the angle between surface normal and ray direction (Lambert's cosine law). Ray directions are sampled similar to the reflected case (formula 4, 5). The distance between radiation source and RPC surface is calculated as the minimum distance between two individual RPC cylinders within a receiver-reactor cavity as described in [7], utilizing the maximum surface fraction $\eta_{\text{surf,max}}$ and assuming a square grid arrangement of the cylinders within the cavity (formula 7). As for both geometries the RPC dimensions parallel to the radiation source are considerably larger compared to the material thickness, the structures are modeled as infinitely long. This allows to reduce the geometrical representation to a two-dimensional cross-section.

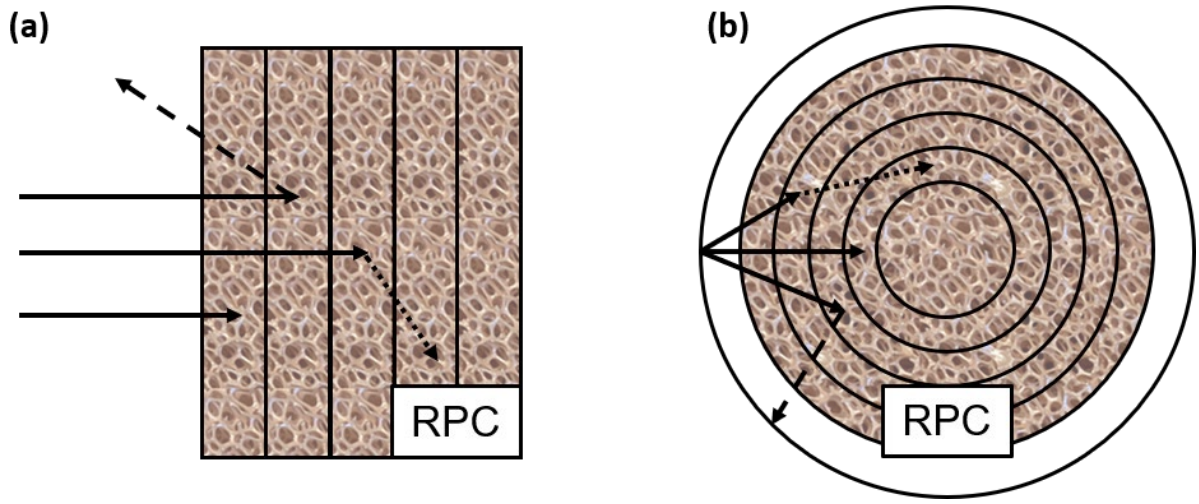

***Figure 2**. Schematic of the two geometries simulated, with discrete spatial RPC elements outlined. Solid arrows indicate incoming rays, dotted arrows reflected rays that are absorbed within the RPC structures and dashed arrows backscattered rays leaving the RPC structures. (a) Flat RPC geometry irradiated from one side by collimated radiation. (b) Cylindrical RPC geometry irradiated from concentric cavity by diffuse radiation.*

2.2 Model validation and simulation parameters

For the simulation setup the spatial discretization of the RPC geometry arranges individual elements circular for the cylinder geometry, while for the flat RPC elements are arranged linear along the material thickness. The spatial step size is selected, such that along the (radial) material thickness $N_{\mathrm{RPC}} = 20$ elements are modeled. This number is selected since the results are expected to be used in a heat transfer model and a mesh study, performed for a 1D transient thermal model for a cylindrical RPC, obtained with 20 elements a variation in the total reduction extent of below 0.5% compared to the converged solution [7]. In order to determine a sufficient number of rays, a ray study is carried out for the range of RPC cylinder radii investigated (figure 3a). The smallest spatial step size ($0.005\ \mathrm{m}$) is used for all radii in the ray study. Based on the results a total number of rays of $N_{\mathrm{ray}} = 5 \times 10^5$ is selected for all simulations, resulting in a relative standard deviation of ray absorptions within the outermost cylinder shell element of below 1%.

In order to validate the model results, simulations are performed that can be compared to analytical solutions. The intensity attenuation along the material thickness is compared to the analytical Beer-Lambert law and numerical view factors are compared to the ratio between cylinder and cavity radii. For validation of the ray propagation length within the RPC structure a directly irradiated, non-scattering ($\alpha_{\mathrm{CeO_{2-\delta}}} = 1.0$), flat RPC geometry is simulated. The relative intensity attenuation along the material thickness is compared to the analytical solution given by the Beer-Lambert law (figure 3b). The numerical intensity attenuation (symbols) for extinction coefficients in the range of $100 - 500\ \mathrm{m^{-1}}$ match well with the analytical solutions (solid lines). For validation of the model geometry and diffuse radiation source, simulations are performed for a perfectly absorbing ($\alpha_{\mathrm{CeO_{2-\delta}}} = 1.0$) opaque ($\beta_{\mathrm{RPC}} = 1 \times 10^6 \mathrm{m^{-1}}$) RPC cylinder. The resulting ratio between total absorbed power by the RPC cylinder and total power diffusely emitted by the cavity is compared to the analytical view factor for two concentric infinitely long cylinders, which is given by the ratio of the inner (RPC) to the outer (cavity) cylinder radius (formula 8). The mean deviation of the numerical values from the analytical view factors for the investigated RPC radii is below 1% ($\approx 0.12\%$).

$$F_{\mathrm{analytical,cavity\rightarrow RPC}} = \frac{r_{\mathrm{RPC}}}{r_{\mathrm{cavity}}}, \qquad F_{\mathrm{numerical,cavity\rightarrow RPC}} = \frac{\dot{Q}_{\mathrm{abs,total}}}{\dot{Q}_{\mathrm{em,total}}} \tag{8}$$

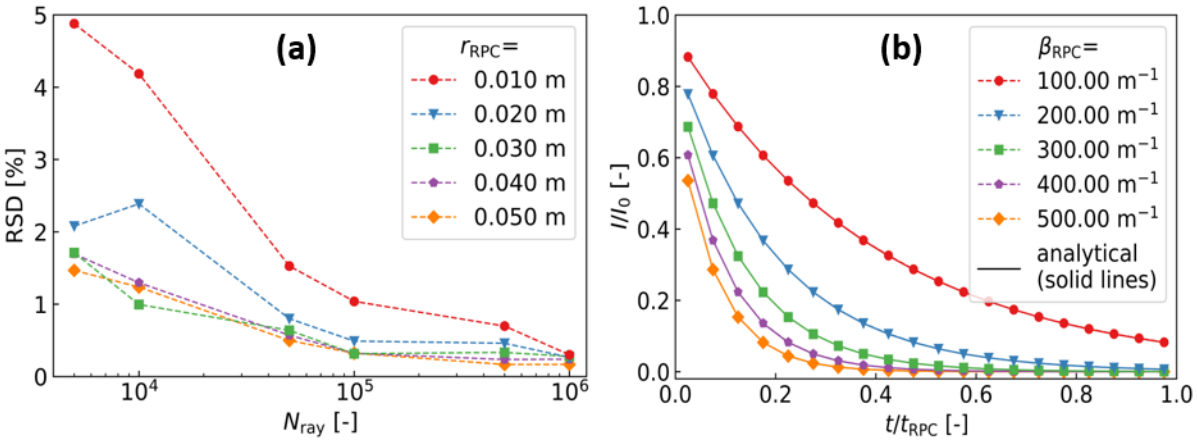

Figure 3. *(a) Relative standard deviation (RSD) of ray absorptions in the outermost RPC cylinder shell element for different RPC radii, plotted against the total number of rays simulated (log-scale). (b) Relative intensity for a perpendicular irradiated non-scattering flat RPC geometry with different extinction coefficients, plotted against the relative material thickness. Intensity values consider the attenuation within the respective elements. Analytical solutions are plotted as solid lines.*

3. Results

3.1 Direct irradiation of flat RPC structure

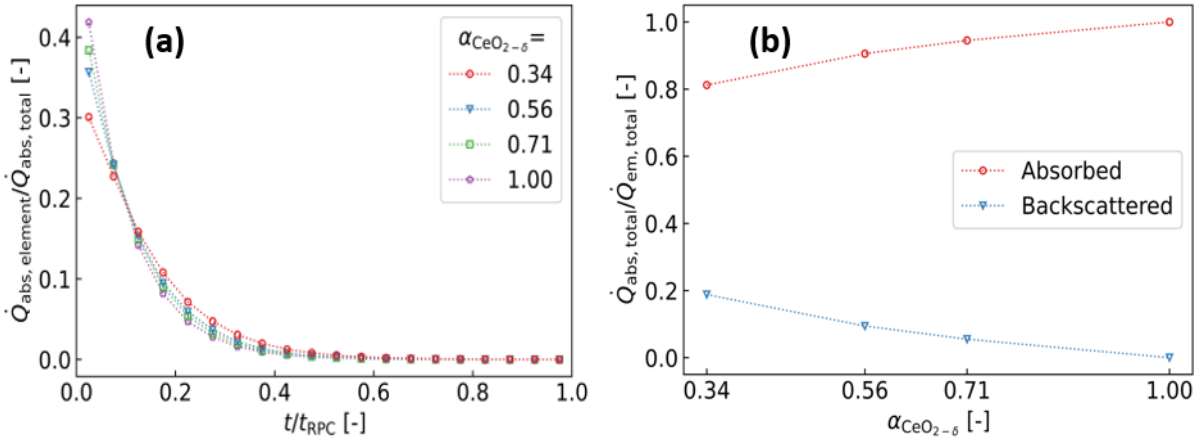

Figure 4. *(a) Absorbed power in flat RPC elements relative to total power absorbed in flat RPC structure for different absorptivity values, plotted against the relative material depth. (b) Total power absorbed by flat RPC structure relative to total incoming radiation power for different absorptivity values.*

For the case of a flat RPC structure that is directly irradiated with collimated radiation, the absorption profiles are shown in figure 4a. The absorption profiles show the power absorbed within each RPC element normalized with respect to the total power absorbed within the RPC structure. The absorption profiles are plotted against the relative material depth within the flat RPC geometry. Different homogeneous values of $\alpha_{CeO_{2-\delta}}$ are selected, representing different reduction states of the redox material. For the lowest values of $\alpha_{CeO_{2-\delta}} = 0.34$ the structure is assumed to be almost fully oxidized ($\delta \approx 0$), for $\alpha_{CeO_{2-\delta}} = 0.56$ the redox material is in the state after oxidation at $T_{ox} = 1200\ \mathrm{K}$ [7] and $\alpha_{CeO_{2-\delta}} = 0.71$ is taken from literature for an average reduction extent of $\delta = 0.035$ [9]. The absorptivity influences the relative absorption profile only slightly. For lower $\alpha_{CeO_{2-\delta}}$ values radiation is scattered deeper into the material or back out of the RPC structure. More apparent is the effect on the total amount of backscattered radiation

shown in figure 4b for the different absorptivity values. For the fully oxidized case approximately 20% of the total amount of incoming radiation is backscattered out of the RPC structure.

3.2 Indirect irradiation of RPC cylinder

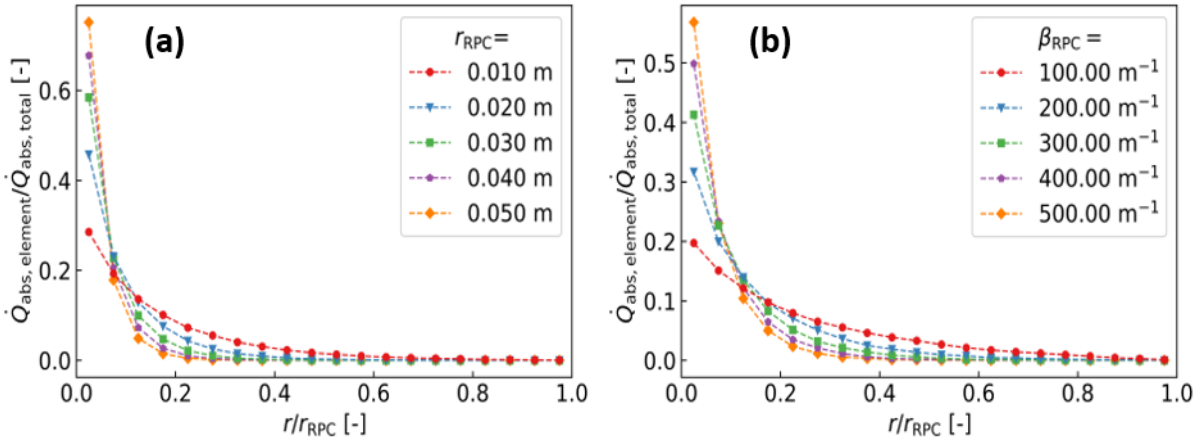

Figure 4. *Absorbed power in cylinder shell elements relative to total absorbed power in RPC cylinder for (a) different RPC radii and (b) different extinction coefficients, plotted against the relative (radial) material depth of the elements.*

Absorption profiles for indirectly (diffuse) irradiated RPC cylinders are shown in figure 4. The graphs show the power absorbed within each cylinder shell element normalized with respect to the total power absorbed within the RPC structure. The absorption profiles are plotted against the relative material depth along the radial direction, with 0 representing the cylinder surface and 1 the center. In figure 4a, the absorption profiles for different RPC radii are shown. For smaller RPC cylinders the absorbed energy is distributed more uniformly along the radial thickness, whereas for larger cylinder radii a large fraction of the absorbed energy is located near the RPC surface. Absorption profiles for different extinction coefficient β_{RPC} are shown in figure 4b. For small extinction coefficients the radiation can penetrate deeper into the material, resulting in a more homogeneous distribution along the material thickness. For β_{RPC} values of $400\mathrm{m}^{-1}$ and more, more than half of the power is absorbed within the outer radial region (10% of radial depth). RPC structures with extinction coefficients in the range of $348.75\ \mathrm{m}^{-1}$ to $413.16\ \mathrm{m}^{-1}$ are reported for reactor models and experiments [9, 12].

4. Summary and outlook

The Monte-Carlo ray-tracing model presented here is a tool that can be used to investigate the volumetric absorption of incoming radiation inside of different porous $\mathrm{CeO}_{2\text{-}\delta}$ structures. Exemplarily volumetric absorption profiles for two cases are presented, one using direct collimated irradiation and one with indirect diffuse radiation. For the direct case a flat RPC geometry is considered, while a cylindrical RPC is irradiated indirectly. Both cases resemble simplifications of redox structures in real reactor designs but capture the volumetric absorption more accurately than in previous 1D simulations [7] and allow to consider local variations of material properties. The results of the simulation are intended to be used as input for heat transfer models in order to improve the accuracy of RPC temperature profile predictions in generic reactor studies. For a proper description of the radiation exchange between a hot reactor environment and the RPC cylinder, reradiation from the RPC itself needs to be considered as well. The model will therefore be extended to simulate radiation originating from within the RPC volume, investigating radiation losses towards the reactor cavity and internal radiation exchange.

Table 2. *Parameter values. Values used for direct irradiation of flat RPC structures are marked with *.*

Parameter	Symbol	Value / Range	Unit	Source
RPC radius, thickness	r_{RPC}, t_{RPC}	0.025	m	[9]
RPC elements	N_{RPC}	20	-	[7]
RPC extinction coefficient	β_{RPC}	435.16	m^{-1}	[9]
$CeO_{2-\delta}$ reduction extent	δ	$0.038, 0.035^{*}$	-	[7, 9]
$CeO_{2-\delta}$ absorptivity	$\alpha_{CeO_{2-\delta}}$	$0.62, 0.7095^{*}$	-	[7, 9]
Radiation source temperature	T_{source}	$1773, 5780^{*}$	K	[9]
Number of rays	N_{ray}	5×10^{5}	-	
Maximum surface fraction	$\eta_{\mathrm{surf,frac}}$	0.15	-	[7]

Data availability statement

Data will be made available on request.

Author contributions

LT: Louis Thomas; **SB**: Stefan Brendelberger; **RTB**: Robin Tim Broeske; **MR**: Martin Roeb; **CS**: Christian Sattler

Conceptualization **SB, LT**; Funding acquisition **SB, MR, CS**; Methodology **LT, SB, RTB**; Resources **SB, MR, CS**; Supervision **SB**; Validation **LT, SB, RTB**; Writing – original draft **LT**; Writing – review & editing **LT, SB, RTB**

Competing interests

The authors declare that they have no competing interests.

Funding

We gratefully acknowledge financial support from the EU HORIZON program (project SUN-to-LIQUID II, grant No. 101122206) and the Swiss State Secretariat for Education, Research and Innovation (SERI).

This work was partially funded by the German Federal Ministry for Economic Affairs and Climate Action under the funding code Redox3D (03EE5124A). The author is responsible for the content of this publication.

References

[1] P. Brandon and Z. Kurban, “Clean energy and the hydrogen economy,” *Philosophical transactions. Series A, Mathematical, physical, and engineering sciences*, vol. 375, no. 2098, 2017, doi: 10.1098/rsta.2016.0400.

[2] M. Romero and A. Steinfeld, “Concentrating solar thermal power and thermochemical fuels,” *Energy Environ. Sci.*, vol. 5, no. 11, p. 9234, 2012, doi: 10.1039/c2ee21275g.

[3] S. Abanades and G. Flamant, “Thermochemical hydrogen production from a two-step solar-driven water-splitting cycle based on cerium oxides,” *Solar Energy*, vol. 80, no. 12, pp. 1611–1623, 2006, doi: 10.1016/j.solener.2005.12.005.

[4] S. Zoller *et al.,* "A solar tower fuel plant for the thermochemical production of kerosene from H2O and CO2," *Joule*, vol. 6, no. 7, pp. 1606–1616, 2022, doi: 10.1016/j.joule.2022.06.012.
[5] M. Hoes, S. Ackermann, D. Theiler, P. Furler, and A. Steinfeld, "Additive-Manufactured Ordered Porous Structures Made of Ceria for Concentrating Solar Applications," *Energy Technol.*, vol. 7, no. 9, p. 1900484, 2019, doi: 10.1002/ente.201900484.
[6] S. Sas Brunser and A. Steinfeld, "Design and Optimization of Hierarchically Ordered Porous Structures for Solar Thermochemical Fuel Production Using a Voxel-Based Monte Carlo Ray-Tracing Algorithm," *ACS Eng. Au*, 2023, doi: 10.1021/acsengineeringau.3c00013.
[7] S. Brendelberger, "R2Mx plant model for solar thermochemical hydrogen production at MW scale," *International Journal of Hydrogen Energy*, Submitted in 2024.
[8] P. Furler and A. Steinfeld, "Heat transfer and fluid flow analysis of a 4kW solar thermochemical reactor for ceria redox cycling," *Chemical Engineering Science*, vol. 137, pp. 373–383, 2015, doi: 10.1016/j.ces.2015.05.056.
[9] S. Zoller, E. Koepf, P. Roos, and A. Steinfeld, "Heat Transfer Model of a 50 kW Solar Receiver–Reactor for Thermochemical Redox Cycling Using Cerium Dioxide," *Journal of Solar Energy Engineering*, vol. 141, no. 2, 2019, doi: 10.1115/1.4042059.
[10] S. Brendelberger, P. Holzemer-Zerhusen, H. von Storch, and C. Sattler, "Performance Assessment of a Heat Recovery System for Monolithic Receiver-Reactors," *Journal of Solar Energy Engineering*, vol. 141, no. 2, 2019, doi: 10.1115/1.4042241.
[11] S. Ackermann, M. Takacs, J. Scheffe, and A. Steinfeld, "Reticulated porous ceria undergoing thermochemical reduction with high-flux irradiation," *International Journal of Heat and Mass Transfer*, vol. 107, pp. 439–449, 2017, doi: 10.1016/j.ijheatmasstransfer.2016.11.032.
[12] S. Brendelberger, P. Holzemer-Zerhusen, E. Vega Puga, M. Roeb, and C. Sattler, "Study of a new receiver-reactor cavity system with multiple mobile redox units for solar thermochemical water splitting," *Solar Energy*, vol. 235, pp. 118–128, 2022, doi: 10.1016/j.solener.2022.02.013.